Enhanced dielectric properties and energy storage density in poly(vinylidene fluoride-co-hexafluoropropylene) by relaxor ferroelectric ceramic

ARTICLE *in* RSC ADVANCES · AUGUST 2015

Impact Factor: 3.84 · DOI: 10.1039/C5RA11753D

6 AUTHORS, INCLUDING:

Hang Luo

Central South University

7 PUBLICATIONS **7** CITATIONS

SEE PROFILE

Chao Chen

Central South University

42 PUBLICATIONS **603** CITATIONS

SEE PROFILE

Xuefan Zhou

Central South University

3 PUBLICATIONS **2** CITATIONS

SEE PROFILE

Dou Zhang

Central South University

101 PUBLICATIONS **500** CITATIONS

SEE PROFILE

RSC Advances

PAPER

View Article Online
View Journal | View Issue

Cite this: RSC Adv., 2015, 5, 68515

Enhancement of dielectric properties and energy storage density in poly(vinylidene fluoride-*co*-hexafluoropropylene) by relaxor ferroelectric ceramics

Hang Luo, Chao Chen, Kechao Zhou,* Xuefan Zhou, Zhong Wu and Dou Zhang*

Received 18th June 2015
Accepted 28th July 2015

DOI: 10.1039/c5ra11753d

www.rsc.org/advances

In this study, a relaxor ferroelectric ceramic, $0.67Pb(Mg_{1/3}Nb_{2/3})O_3$–$0.33PbTiO_3$ (PMN–PT), was synthesized by a molten-salt growth method with lower remnant polarization and slimmer hysteresis loops than traditional ferroelectric ceramics. The PMN–PT particles remained homogeneously dispersed in the composite and adhered tightly to a poly(vinylidene fluoride-*co*-hexafluoropropylene) (P(VDF-HFP)) matrix due to the modification of the particles with dopamine. The composites had a maximum dielectric constant of 65.1 and a low dielectric loss of less than 0.037 at 1 kHz. Due to the low remnant polarization of the relaxor ferroelectric ceramic of PMN–PT, the energy density of the composites significantly increased. The discharged energy density of the sample with 50 vol% PMN–PT was 4 times that of P(VDF-HFP) at 80 kV mm^{-1}. It was demonstrated that the dopamine functionalized PMN–PT/P(VDF-HFP) composite was a potential dielectric material with potential future applications in energy storage.

Introduction

Dielectric materials with high discharged energy densities have attracted scientific and commercial interest due to the prospect of their application in electronic devices such as radar, lasers, defibrillators, rail guns, and pacemakers.[1–5] However, the technology in its current state suffers from low energy density, which makes the materials bulky and costly. One desirable strategy to increase the energy density of these materials is to apply 0–3 type inorganic/polymer composites (zero-dimensional fillers in a three-dimensionally connected polymer matrix), because they have high dielectric strength; also, the polymer confers excellent processability, which helps overcome the limitations associated with conventional inorganic ceramic and organic dielectric materials.[6–13] In general, the discharged energy density (J) of a dielectric material is related to this equation:

$$J = \int_{D_r}^{D_{max}} E \mathrm{d}D \quad (1)$$

where D_{max} and D_r are the maximum electric displacement and remnant electric displacement of the materials, respectively, and E is the applied electric field. Electric displacement (D) is defined as:

$$D = \varepsilon_0 \varepsilon_r E \quad (2)$$

where ε_0 and ε_r are the dielectric constant of a vacuum and the relative dielectric constant of the dielectric material, respectively. It can be seen that J can be increased by simultaneously increasing the dielectric constant and the breakdown strength.[14,15] Thus, finding a material with a high dielectric constant and dielectric strength without a large increase in dielectric loss is the key factor to promote the development of dielectric materials for energy storage applications.[16]

In general, ferroelectric ceramics, such as Pb(Zr, Ti)O_3 (PZT), and $BaTiO_3$, have often been chosen for use as fillers in polymer composites due to their high dielectric constants.[17–19] However, ferroelectric ceramics always suffer from fat hysteresis loops with high coercive electric fields and high remanent polarization, which decreases the discharged energy density and energy efficiency.[20–22] In contrast, relaxor ferroelectric ceramics, such as (Ba, Sr)TiO_3, La-doped PZT, and $Pb(Mg_{1/3}Nb_{2/3})O_3$–$PbTiO_3$ (PMN–PT), exhibit higher dielectric constants, relatively low remnant polarization and slim hysteresis loops in comparison to traditional ferroelectric ceramics.[22,23] Recently, relaxor ferroelectric ceramics have received a great deal of attention for energy storage applications. Brown *et al.* reported the use of a relaxor ferroelectric ceramic, La-doped PZT, for energy storage applications. Due to the relatively low remanent polarization and coercive electric field, a maximum energy density of 13.3 J cm^{-3} with an energy efficiency of 77% was obtained.[24] Similarly, Hao *et al.* achieved a maximum energy density of 28.7 J cm^{-3} in La-doped PZT films with a thickness of 1 μm on platinum-buffered silicon substrates.[25] Wu *et al.* reported a novel relaxor

State Key Laboratory of Powder Metallurgy, Central South University, Changsha, Hunan 410083, China. E-mail: dzhang@csu.edu.cn; zhoukechao@csu.edu.cn

ferroelectric capacitor of $BaTiO_3$@$SrTiO_3$ ceramic with a core–satellite structure, which largely enhanced the energy storage density and improved energy efficiency compared with ferroelectric $BaTiO_3$.[26] Much attention has been paid to relaxor ferroelectric ceramics for energy storage; however, flexible relaxor ferroelectric ceramic/polymer composites with the high dielectric constants of relaxor ceramics and the high dielectric strengths of polymer matrices have been overlooked. Therefore, introducing relaxor ferroelectric ceramics into a polymer matrix could be useful to prepare flexible dielectric materials with improved discharged energy densities and energy efficiencies.

In this study, relaxor ferroelectric PMN–PT ceramic particles were synthesized by a molten-salt growth method. The synthesized PMN–PT ceramic particles were modified with dopamine before being introduced to a poly(vinylidene fluoride-*co*-hexafluoropropylene) (P(VDF-HFP)) matrix. Compared with the pristine PMN–PT, the modified PMN–PT particles dispersed homogeneously in the composites and showed strong interfacial adhesion to the polymer matrix; moreover, the composite with the modified PMN–PT particles showed improved dielectric properties. The energy density storage of the composites was as high as 1.02 J cm^{-3}, which is more than four times greater than that of the pure P(VDF-HFP) matrix. The findings of this research could provide an effective approach to build high energy density storage capacitors.

Experimental section

Materials

The chemicals were obtained from the following sources and used without further purification: PbO (Kermel, China, 99%), Nb_2O_5 (Sinopharm, China, 99%), $[(MgCO_3)_4Mg(OH)_2]5H_2O$ (Sinopharm, China, 99%), TiO_2 (Anatase, Aladdin, 99.8%), and KCl (Sinopharm, China, 99.5%). Dopamine hydrochloride (Alfa, 99%), P(VDF-HFP) (Aldrich, pellets with less than 15% of HFP), and other reagents were all analytically pure.

Synthesis of PMN–PT powders by molten-salt growth method

11.5 g of PbO (51.5 mmol, excess 3%), 1.07 g of $[(MgCO_3)_4Mg(OH)_2]5H_2O$ (2.2 mmol), 2.95 g of Nb_2O_5 (11.1 mmol), 1.33 g of TiO_2 (16.7 mmol) and 17 g of KCl (228.2 mmol) were mixed in ethyl alcohol by ball-milling with a speed of 150 rpm for 12 h. The mass ratio of the raw material, media and ball was 1 : 1 : 1.5. The sintering process was performed at 850 °C for 1 h; afterwards, the product was soaked in water at 80 °C for 24 h. The soaked content underwent heat treatment at 650 °C for 1 h after suction filtration. PMN–PT powder, with a composition of $0.67Pb(Mg_{1/3}Nb_{2/3})O_3$–$0.33PbTiO_3$, was finally obtained by planetary ball-milling for 4 days.

Functionalization of the PMN–PT particles

Dopamine modified PMN–PT was prepared using a method reported previously.[27] In a typical reaction, 10 g of PMN–PT particles was dispersed in 100 mL of a mixture of 95 : 5 (v/v) ethanol/H_2O using an ultrasonic processor to increase the hydroxyl groups on the surface of the PMN–PT. The PMN–PT particles were recovered by centrifugation and dried under vacuum at 60 °C for 12 h. The hydroxylated PMN–PT particles were dispersed in 0.01 M dopamine hydrochloride aqueous solution and stirred for 10 h at 60 °C. The particles were separated by centrifugation and rinsed repeatedly with excess deionized water. Afterwards, the functionalized PMN–PT particles were dried overnight under vacuum at 60 °C.

Fabrication of the PMN–PT/P(VDF-HFP) composites

Functionalized PMN–PT particles were ball-milled in *N*,*N*-dimethylformamide (DMF) for 2 days and mixed with P(VDF-HFP) for another 5 days by ball-milling. The resulting suspension was then casted onto a clean glass and dried at 80 °C for 12 h under vacuum. The dried composite sheets were compressed into films at 200 °C under a pressure of about 15 MPa. Gold electrodes were sputtered on both sides of the film using a mask with 2 mm diameter eyelets.

The fabrication process of the PMN–PT/P(VDF-HFP) composites is shown in Fig. 1. As the image shows, the PMN–PT particles were first modified with dopamine. The chemical structure of dopamine contains OH groups and NH_2, which can interact strongly with a variety of inorganic particles by hydrogen bonding.[28] In addition, dopamine could form strong covalent and noncovalent interactions with the substrates.[29] As shown, the polymerization reaction of dopamine took place on the surface of the particles.[30–32] The functional PMN–PT particles were then dispersed in the P(VDF-HFP) solution by ball-milling. The modifier adhered tightly on the surface of the PMN–PT particles; meanwhile, the organic layer bonded tightly with the polymer matrix due to the presence of a strongly electron-withdrawing functional group (–C–F) on P(VDF-HFP). Afterwards, the composite films were prepared as reported previously.[7]

Characterization

The crystal structures of the ceramic and composites were examined in θ–2θ mode by X-ray diffraction (XRD, Rigaku D-Max/2550VB$^+$) utilizing Cu K_α radiation ($\lambda = 1.5418$ Å). Fourier-transform infrared (FT-IR) spectroscopy was performed with a Nicolet 6700 instrument over the range of 4000 to 450 cm^{-1} to determine the functionalization of the samples. Transmission

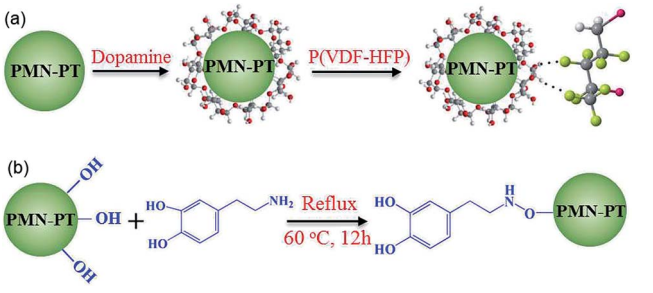

Fig. 1 Schematic of (a) modified PMN–PT particles by dopamine in the P(VDF-HFP) composite and (b) the reaction between the PMN–PT particles and dopamine.

electron microscopy (TEM) images were obtained from a Titan G2 60-300 instrument operated at an accelerating voltage of 300 kV. Thermogravimetric analysis (TGA, NETZSCH STA 449) was conducted at a heating rate of 10 °C min^{-1} under a nitrogen flow (20 mL min^{-1}). The morphology of the composites was determined by scanning electron microscopy (SEM, JSM-6390). The frequency-dependent dielectric constant and dielectric loss were measured using an Agilent 4294A LCR meter with a frequency range from 100 Hz to 10 MHz. The electric displacement–electric field loops and leakage current were measured by a Precision Premier II ferroelectric polarization tester (Radiant, Inc.) at room temperature and 100 Hz.

Results and discussion

Characterization of pristine PMN–PT and dopamine modified PMN–PT particles

Fig. 2 exhibits the X-ray diffraction pattern of the PMN–PT particles. It is shown that the strong peaks at 2θ of 22, 31, 39, 45, 51, and 56 can be attributed to the (100), (110), (111), (200), (210) and (211) characteristic peaks of PMN–PT with cubic crystalline. All of the peaks matched well with the perovskite peaks found in the powder diffraction file database (#80-1351). These peaks indicated that a pure perovskite phase was obtained in the PMN–PT particles by the molten-salt growth method. The morphologies of the PMN–PT particles were revealed by SEM, and the image is shown in Fig. 2. As can be seen, the particles had irregular shapes and wide size distribution. The average diameter was about 320 nm and was measured by a laser particle size analyzer. The results were attributed to the limitations of mechanical ball-milling.

The FT-IR absorbance spectra of the pristine PMN–PT particles, the dopamine modified PMN–PT particles, and pure dopamine is shown in Fig. 3. The absorption intensity in the range of 3800 to 800 cm^{-1} increased after the PMN–PT particles were modified by dopamine. A broad absorbance band between 3500 and 3000 cm^{-1} appeared after the surface modification, which corresponds to O–H and/or N–H stretching vibrations derived from dopamine.[33] The absorption peaks located at 1616 and 1286 cm^{-1} are due to N–H bending vibrations and aromatic amine C–N stretching vibrations, respectively, which originate from the aromatic and amino groups. Meanwhile, these absorption peaks did not appear in the sample of the pristine PMN–PT particles. In addition, the absorption peak located at 1680 cm^{-1} only appeared in the sample of dopamine modified PMN–PT, which indicated that a new covalent N–O bond was formed. The results implied that dopamine was attached to the surface of the functionalized PMN–PT particles.

Fig. 4a displays the TEM image of the PMN–PT particle functionalized with dopamine. A polymer layer with a thickness of ~7 nm can be clearly observed on the surface of the PMN–PT particle. The corresponding high-resolution image of the functionalized PMN–PT particle is exhibited in Fig. 4b. An obvious interface with a discrepant high resolution stripe can be seen in the two sides of the interface, which agrees with the result in Fig. 4a. Fig. 4c shows the TGA curves of pristine PMN–PT, functionalized PMN–PT particles, and pure dopamine. The amount of dopamine coated on the surfaces of the PMN–PT particles was characterized by TGA. The net weight loss of functionalized PMN–PT was found to be 3.2%; this was attributed to the coated dopamine, because the weight loss of pure dopamine was about 75%, while the pristine PMN–PT almost had no weight loss.

Characterization of the PMN–PT/P(VDF-HFP) composites

The microscopic homogeneity of the PMN–PT/P(VDF-HFP) composite films was investigated by imaging the cross sections, which are shown in Fig. 5. In the SEM images, the content of the PMN–PT particles in samples (a), (b) and (c) were 10 vol%, 30 vol% and 50 vol%. Samples (d), (e) and (f) had the same PMN–PT content as samples (a), (b) and (c); the difference was that the PMN–PT particles in samples (d), (e) and (f) were modified with dopamine before being introduced to the polymer matrix. A small number of particles were observed in the composites when the content of PMN–PT was 10 vol%, which is shown in Fig. 5a and d. The visible particles in the composites

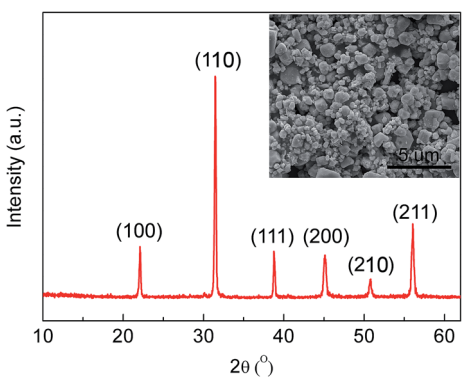

Fig. 2 X-ray diffraction pattern of the PMN–PT ceramic particles. The inset is a SEM image of the PMN–PT particles.

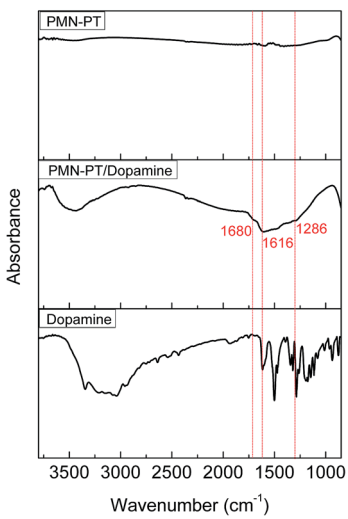

Fig. 3 The FT-IR spectra of PMN–PT, modified PMN–PT by dopamine and pure dopamine.

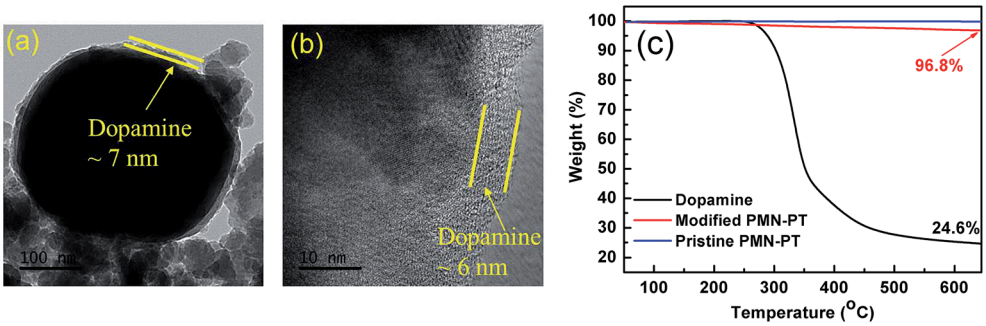

Fig. 4 (a) Bright-field image and (b) HR-TEM image of a PMN–PT particle after surface modification with dopamine. (c) TGA curves for the pristine PMN–PT, modified PMN–PT by dopamine, and pure dopamine.

became more and more intensive with increasing loading of PMN–PT. It can be clearly seen that the unmodified PMN–PT exhibited poor compatibility with the P(VDF-HFP) matrix; the particles were scattered in the matrix without a bonding force, and an increasing number of defects were found in the composites as the PMN–PT loading increased. Satisfyingly, these problems distinctly decreased after the PMN–PT particles were modified with dopamine. As can be seen in Fig. 5d–f, the particles were uniformly embedded in the polymer matrix with a strong bonding force, and negligible evidence of defects was observed even when the loading of PMN–PT reached 50 vol%. Larger interfacial areas between the polymer matrix and the particles in the composites than the unmodified particles were achieved, which can promote the coupling effect through a dipolar interface layer and result in higher polarization and dielectric response.[33,34] Thus, PMN–PT modified with dopamine is beneficial to enhance the dielectric properties and energy storage capacity of the composite.

Fig. 6a shows the XRD patterns of pure P(VDF-HFP) and PMN–PT/P(VDF-HFP) composites with different amounts of PMN–PT. It can be seen that the XRD pattern of the pure P(VDF-HFP) exhibited an intense scattering background and a wide hump at about 20°, which are typical features of an amorphous structure. Both the diffraction peaks from the perovskite structure of the PMN–PT ceramics and the scattering hump from the P(VDF-HFP) matrix can be observed in the composite films. The XRD pattern of the composites showed diffraction peaks located at 22°, 31°, and 39°, which can be attributed to the (100), (110), and (111) reflections of PMN–PT (no. #80-1351). However, as shown in the dotted box, the diffraction peaks of P(VDF-HFP) became increasingly negligible in the composites as the PMN–PT loading increased. This result indicated that the introduction of PMN–PT particles destroyed the crystallization of the P(VDF-HFP) matrix, and the amorphous degree increases with increasing PMN–PT particle loading.[35] The DSC curves of the samples obtained during the heating scan process are presented in Fig. 6b. It can be seen that the crystallization temperature increased by 4.5 °C with the introduction of the PMN–PT particles, from 155.9 °C for the P(VDF-HFP) to 160.4 °C for the composite with 10 vol% PMN–PT particles. However, the crystallization temperature decreased with increasing PMN–PT loading. The PMN–PT fillers affect the crystallization

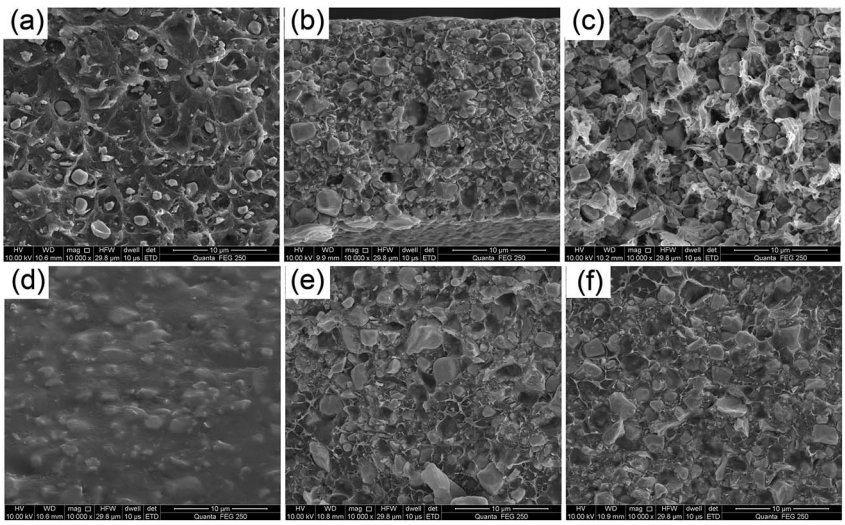

Fig. 5 SEM images of cross sections of the composites with (a) 10 vol%, (b) 30 vol%, (c) 50 vol% PMN–PT particles, and (d) 10 vol%, (e) 30 vol%, (f) 50 vol% dopamine modified PMN–PT particles.

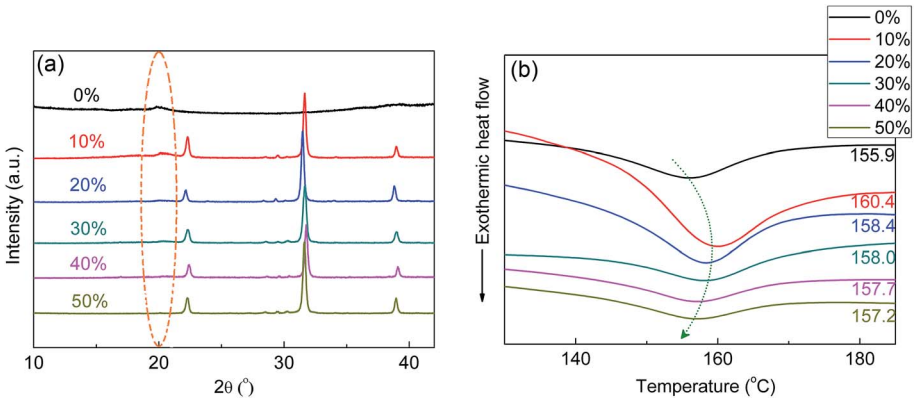

Fig. 6 (a) XRD patterns of PMN–PT particles, pure P(VDF-HFP), and PMN–PT/P(VDF-HFP) composites with different volume fractions of BT. (b) DSC curves of the samples during the heating cycle at a rate of 10 °C min under N_2 atmosphere.

temperature of the P(VDF-HFP) composites mainly due to two reasons. One reason is that the PMN–PT fillers in the composite act as the new nucleation center, which can decrease the nucleation energy and increase the degree of crystallization of the P(VDF-HFP) matrix for the crystallization of P(VDF-HFP) on the surface of PMN–PT. Another reason is that the introduction of PMN–PT fillers decreased the degree of order of the P(VDF-HFP) matrix, which means that the degree of crystallization of the P(VDF-HFP) matrix decreased. Thus, the crystallization temperature of P(VDF-HFP) increased with small amounts of PMN–PT particles, while it decreased as the particle loading increased.

Dielectric properties and energy storage performance of the PMN–PT/P(VDF-HFP) composites

To further discuss the effect produced by dopamine on the dielectric properties, the frequency dependence of the dielectric properties of the compared composites with unmodified PMN–PT and modified PMN–PT, respectively, are shown over the range of 100 Hz to 100 MHz; this is exhibited in Fig. 7. As can be seen, the composites with modified PMN–PT fillers had improved dielectric properties compared to the composites with unmodified PMN–PT fillers. The maximum dielectric constant of the composite with modified PMN–PT increased from 8.3 to 65.1, while that of the composite with unmodified fillers was 53.5. The high dielectric constant of the composites mainly arose from the MWS interfacial effect;[36] the PMN–PT fillers modified with dopamine exhibited uniform dispersion in the composite, which resulted in larger interfacial areas between the PMN–PT particles and the P(VDF-HFP) matrix than in the composite with unmodified fillers. It was noted that the composites with modified PMN–PT had an extremely low dielectric loss of less than 0.037 at 1 kHz at room temperature. The changing trend of the dielectric loss in the high frequency range was the same with the degree of crystallinity of the polymer matrix, which increased at first and then decreased, as shown in Fig. 6b and 7d. The dielectric loss of the composites with unmodified PMN–PT obviously increased, and even increased to 0.103 for the composite with 50 vol% unmodified PMN–PT. This result can be understood from the results of the comparison in Fig. 5, which shows numerous voids and defects in the composite with unmodified PMN–PT.

The effective dielectric constant (at 1 kHz) of the composites as a function of the volume fraction of the PMN–PT particles compared with the predicted values from different theoretical models is shown in Fig. 7e. The experimental dielectric constant gradually increased with increasing filler volume fraction. A large discrepancy between the experimental values and the calculated values from the Maxwell–Garnett model was observed when the particle content was more than 20 vol%. This is due to the interaction among the particles, which becomes increasingly important with increasing PMN–PT particle content. However, the experiment results agree well with the value from the Jayasundere–Smith model.

Fig. 7f shows the frequency dependence of the electrical conductivity for the composites with modified PMN–PT fillers. The samples showed relatively low electrical conductivity, especially when the loading of the PMN–PT fillers was 10 vol% and 20 vol%; the value was even lower than that of pure P(VDF-HFP). The reason was attributed to the dopamine insulating shell on the surface of the PMN–PT particles, which restricted the migration and accumulation of the space charge within the composite. However, the electrical conductivity of the composite increased obviously when the loading of PMN–PT was larger than 20 vol%. For example, the electrical conductivity of the sample with 10 vol% PMN–PT was 1.8×10^{-6} S m^{-1}, and the sample with 50 vol% PMN–PT was 9.3×10^{-6} S m^{-1} at 1 kHz. Unavoidable defects, such as agglomerations, voids and cracks, were produced in the composites when the loading of PMN–PT was high, which lead to the increase of the electrical conductivity.

The frequency dependence of the imaginary electric modulus (M'') of the composites

$$M'' = \varepsilon''/(\varepsilon'^2 + \varepsilon''^2) \quad (3)$$

and the pure P(VDF-HFP) at room temperature are shown in Fig. 8, where ε' and ε'' correspond to the real and imaginary parts of the complex dielectric constant of the samples,

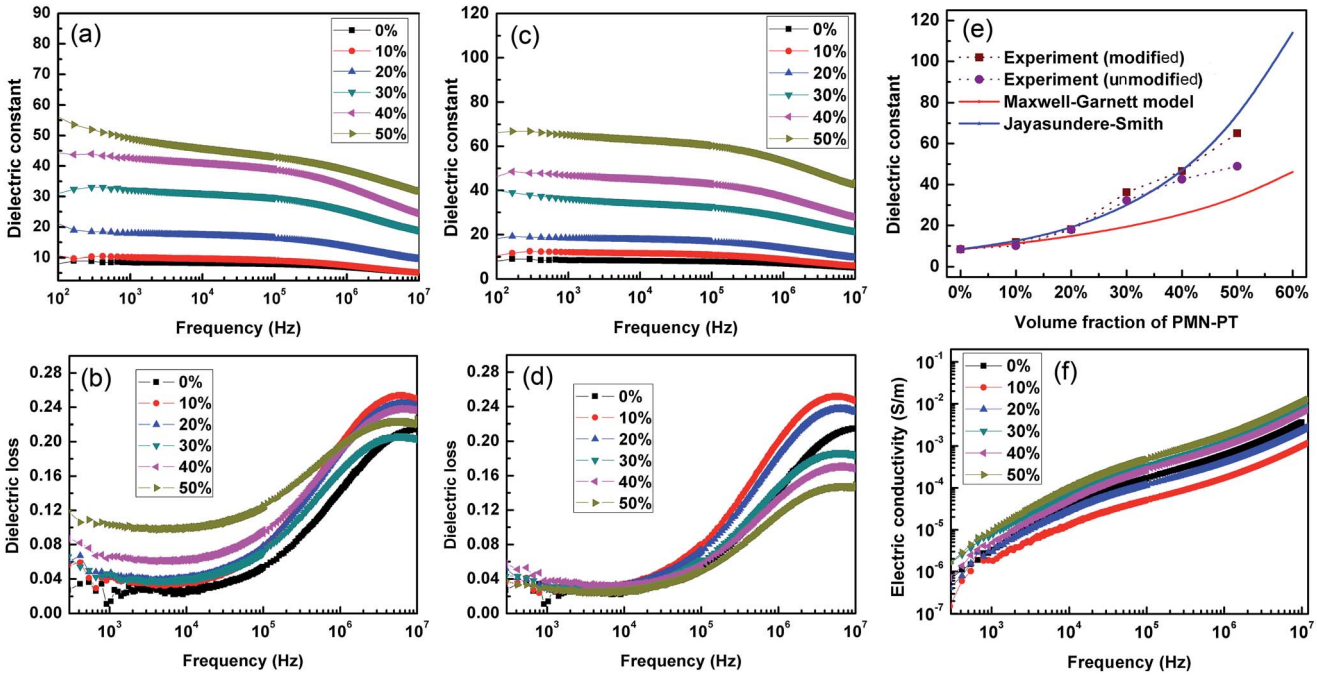

Fig. 7 Frequency dependence of the (a) dielectric constant and (b) dielectric loss of the P(VDF-HFP) composites with unmodified PMN–PT; (c) dielectric constant, (d) dielectric loss, and (f) electrical conductivity of the P(VDF-HFP) composites with modified PMN–PT at room temperature. (e) Comparison of the measured effective relative dielectric constants (at 1 kHz) of the composites as a function of PMN–PT particle volume fraction with predicted values from different theoretical models.

respectively. The relaxation intensity of the samples decreased and broadened with the introduction of PMN–PT compared to P(VDF-HFP), which was especially obvious when the PMN–PT content reached 30 vol%. This result was due to the restraint of the space charge aggregation in the composites by the PMN–PT fillers,[37] and is consistent with the low conductivity of the composites shown in Fig. 7c. The relaxation peaks appeared at a high frequency range ($\sim 10^7$ Hz), which can be attributed to the movement and accumulation of free charges resulting from dipole relaxation of the P(VDF-HFP) matrix at the high frequency range,[7,38] and agreed with the trend of the dielectric loss. Moreover, the peaks shifted to a lower frequency range with increasing PMN–PT content. For example, the relaxation peak of the sample with 10% PMN–PT content was at about 2×10^7 Hz, and moved to about 9×10^6 Hz when the PMN–PT content was increased to 50 vol%.

Discharged energy density is related not only to the dielectric constant but also the breakdown strength of the composite. The results in Fig. 9 show a comparison of the breakdown strengths of the composites with PMN–PT modified with dopamine and unmodified PMN–PT as a function of the loading of PMN–PT. The composites with modified PMN–PT particles have a higher breakdown strength than the composites with unmodified PMN–PT. The breakdown

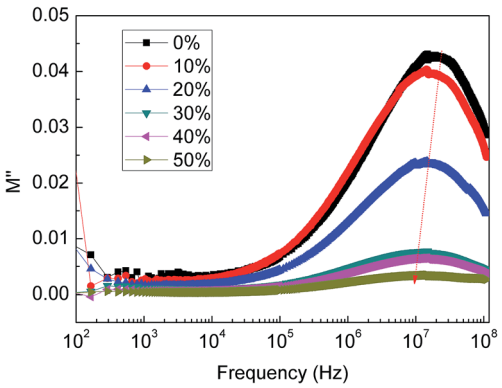

Fig. 8 Frequency dependence of the imaginary electric modulus of the samples with varying PMN–PT particle content at room temperature.

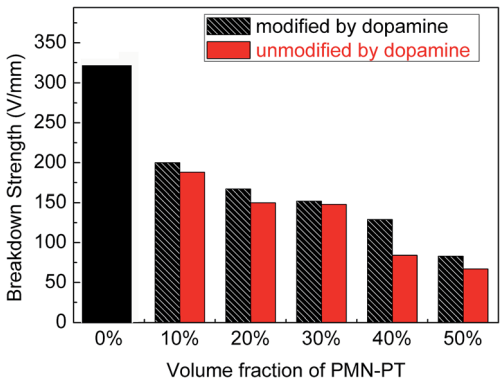

Fig. 9 The comparison of breakdown strength between the composites with modified PMN–PT by dopamine and unmodified PMN–PT as a function of the loading of PMN–PT.

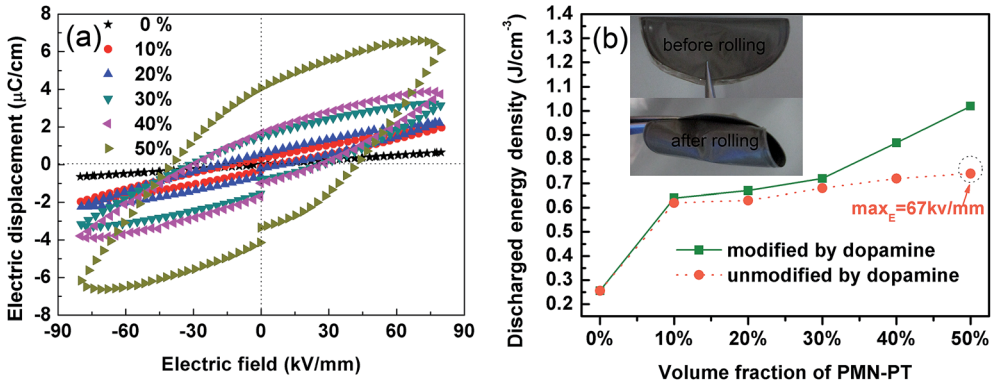

Fig. 10 (a) D–E loops and (b) discharged energy densities of the samples at the electric field of 80 kV mm^{-1}. The difference in the electric field of the composite with 50 vol% unmodified PMN–PT is 67 kV mm^{-1}. The inset in (b) shows the digital image of the flexible composite before rolling and after rolling.

strengths of the composites with modified PMN–PT, in order, were 200, 167, 152, 129, and 83 kV mm^{-1}. For comparison, the breakdown strengths of the composites with unmodified PMN–PT were 188, 150, 148, 74, and 67 kV mm^{-1}. These can be attributed to the superior quality of the composite films after modification with dopamine. As Fig. 5 clearly shows, the modified composite films had no obvious aggregation and ignorable defects. In addition, the breakdown strength decreased with increasing PMN–PT loading; the breakdown strength was 325 kV mm^{-1} for the pure P(VDF-HFP), decreased to 152 kV mm^{-1} for the composite with 30 vol% PMN–PT particles, and decreased further to 83 kV mm^{-1} when the loading of PMN–PT increased to 50 vol%. A similar phenomenon was also observed in the composites with unmodified PMN–PT. The agglomerations and voids in the composites increased in number with increasing PMN–PT, which resulted in inhomogeneous electric field breakdown strength in the polymer matrix and led to the decrease of the effective breakdown strength of the composites.[39,40]

According to eqn (1), J can be derived from the electric displacement–electric field (D–E) loops.[41,42] Typical D–E loops of the composites with various volume fractions of modified PMN–PT particles were measured at the electric field of 80 kV mm^{-1}, and are shown in Fig. 10a. It can be seen that the electric displacement increased notably with increasing PMN–PT filler loading. The detailed performances of the composites originating from the D–E loops are shown in Table 1. It can be seen that the electric displacements of the samples were 0.64, 1.94, 2.25, 3.26, 3.86, and 6.61 μC cm^{-2}. According to eqn (2), the increased electric displacement was due to the increase of the dielectric constant of the samples, which is consistent with the results in Fig. 7c.

Table 1 The performances of the composites containing PMN–PT particles modified with dopamine at the electric field of 80 kV mm^{-1}

No.	D_{max} (μC cm^{-2})	D_r (μC cm^{-2})	U_{max} (J cm^{-3})
0%	0.64	0.01	0.25
10%	1.94	0.32	0.64
20%	2.25	0.57	0.67
30%	3.26	1.47	0.72
40%	3.86	1.69	0.86
50%	6.61	4.06	1.02

The energy density of the samples as a function of PMN–PT filler loading is shown in Fig. 10b. As can be seen, the energy density increased with increasing PMN–PT filler content. The energy density of pure P(VDF-HFP) was 0.25 J cm^{-3} at 80 kV mm^{-1}, and it increased to 1.02 J cm^{-3} when the PMN–PT loading increased to 50 vol% in the same electric field, which is an increase of about 4 times. This is due to the improved dielectric properties of the composites with modified PMN–PT fillers, which led to higher energy densities than the composites with unmodified PMN–PT. Additionally, the PMN–PT/P(VDF-HFP) composite films exhibited excellent flexibility, which can be demonstrated by the digital photo inserted in Fig. 10b. Although relaxor ferroelectric properties were not exhibited by the samples, the use of relaxor ferroelectric ceramics (PMN–PT, BST, *etc.*) composites with polymers for energy storage applications still deserves further study.

Conclusions

Relaxor ferroelectric ceramic PMN–PT ceramics were synthesized and introduced into the ferroelectric polymer P(VDF-HFP). The modified PMN–PT particles maintained homogeneous dispersion in the composite and adhered tightly to the P(VDF-HFP) matrix. Due to the high-quality composite films, the composites with modified PMN–PT exhibited significantly enhanced dielectric properties and energy storage density compared with pure P(VDF-HFP) and the composites with unmodified PMN–PT. The maximum dielectric constant of the composites was as high as 65.1, compared to a value of 8.3 for P(VDF-HFP) at 1 kHz. Meanwhile, the increased dielectric constant was not achieved at the expense of increasing dielectric loss. The composite with 50 vol% modified PMN–PT held 4 times more energy density than P(VDF-HFP) at 80 kV mm^{-1}. The results obtained in this study would be helpful in exploring potential dielectric materials in applications for energy storage.

The manuscript was written with contributions from all the authors. All the authors have given approval to the final version of the manuscript.

Acknowledgements

This work was financially supported by Graduate Student Research Innovation Project in Hunan Province (no. 150140011), Ph.D. Programs Foundation of Ministry of Education of China (no. 20110162110044), and State Key Laboratory of Powder Metallurgy, Central South University, Changsha, China.

References

1 S. Liu, S. Xue, W. Zhang, J. Zhai and G. Chen, *J. Mater. Chem. A*, 2014, **2**, 18040–18046.
2 H. Tang and H. A. Sodano, *Nano Lett.*, 2013, **13**, 1373–1379.
3 B. Chu, X. Zhou, K. Ren, B. Neese, M. Lin, Q. Wang, F. Bauer and Q. M. Zhang, *Science*, 2006, **313**, 334–336.
4 Z. D. Liu, Y. Feng and W. L. Li, *RSC Adv.*, 2015, **5**, 29017–29021.
5 V. K. Thakur, G. Ding, J. Ma, P. S. Lee and X. Lu, *Adv. Mater.*, 2012, **24**, 4071–4096.
6 H. Luo, D. Zhang, C. Jiang, X. Yuan, C. Chen and K. Zhou, *ACS Appl. Mater. Interfaces*, 2015, **7**, 8061–8069.
7 S. Wu, W. Li, M. Lin, Q. Burlingame, Q. Chen, A. Payzant, K. Xiao and Q. M. Zhang, *Adv. Mater.*, 2013, **25**, 1734–1738.
8 V. K. Thakur, E. J. Tan, M.-F. Lin and P. S. Lee, *J. Mater. Chem.*, 2011, **21**, 3751–3759.
9 D. Yuan, Z. Li, W. Thitsartarn, X. Fan, J. Sun, H. Lia and C. He, *J. Mater. Chem. C*, 2015, **3**, 3708–3713.
10 M.-F. Lin, V. K. Thakur, E. J. Tan and P. S. Lee, *J. Mater. Chem.*, 2011, **21**, 16500–16504.
11 V. K. Thakur, M.-F. Lin, E. J. Tan and P. S. Lee, *J. Mater. Chem.*, 2012, **22**, 5951–5959.
12 V. K. Thakur, J. Yan, M.-F. Lin, C. Zhi, D. Golberg, Y. Bando, R. Sim and P. S. Lee, *Polym. Chem.*, 2012, **3**, 962–969.
13 V. K. Thakur, E. J. Tan, M.-F. Lin and P. S. Lee, *Polym. Chem.*, 2011, **2**, 2000–2009.
14 K. Yang, X. Huang, Y. Huang, L. Xie and P. Jiang, *Chem. Mater.*, 2013, **25**, 2327–2338.
15 H. Tang, Y. Lin and H. A. Sodano, *Adv. Energy Mater.*, 2012, **2**, 469–476.
16 C. Ehrhardt, C. Fettkenhauer, J. Glenneberg, W. Münchgesang, H. S. Leipner, G. Wagner, M. Diestelhorst, C. Pientschke, H. Beige and S. G. Ebbinghaus, *RSC Adv.*, 2014, **4**, 40321–40329.
17 H. Luo, D. Zhang, L. Wang, C. Chen, J. Zhou and K. Zhou, *RSC Adv.*, 2015, **5**, 52809–52816.
18 Y. Zhang, G. Gao, H. L. W. Chan, J. Dai, Y. Wang and J. Hao, *Adv. Mater.*, 2012, **24**, 1729–1735.
19 X. Fu, I. I. Naumov and H. Fu, *Nano Lett.*, 2013, **13**, 491–496.
20 O. Auciello, J. F. Scott and R. Ramesh, *Phys. Today*, 1998, **51**, 22–27.
21 H. X. Tang and H. A. Sodano, *Appl. Phys. Lett.*, 2013, **102**, 063901.
22 S. Tong, B. Ma, M. Narayanan, S. Liu, R. Koritala, U. Balachandran and D. Shi, *ACS Appl. Mater. Interfaces*, 2013, **5**, 1474–1480.
23 R. E. Cohen, *Nature*, 2006, **441**, 941–942.
24 E. Brown, C. Ma, J. Acharya, B. Ma, J. Wu and J. Li, *ACS Appl. Mater. Interfaces*, 2014, **6**, 22417–22422.
25 X. Hao, Y. Wang, J. Yang, S. An and J. Xu, *J. Appl. Phys.*, 2012, **112**, 114111.
26 L. Wu, X. Wang, H. Gong, Y. Hao, Z. Shen and L. Li, *J. Mater. Chem. C*, 2015, **3**, 750–758.
27 Y. Song, Y. Shen, H. Liu, Y. Lin, M. Li and C.-W. Nan, *J. Mater. Chem.*, 2012, **22**, 8063–8068.
28 M.-F. Lin, V. K. Thakur, E. J. Tan and P. S. Lee, *RSC Adv.*, 2011, **1**, 576–578.
29 H. Lee, S. M. Dellatore, W. M. Miller and P. B. Messersmith, *Science*, 2007, **318**, 426–430.
30 Q. Yue, M. Wang, Z. Sun, C. Wang, C. Wang, Y. Deng and D. Zhao, *J. Mater. Chem. B*, 2013, **1**, 6085–6093.
31 C. Chao, J. Liu, J. Wang, Y. Zhang, B. Zhang, Y. Zhang, X. Xiang and R. Chen, *ACS Appl. Mater. Interfaces*, 2013, **5**, 10559–10564.
32 B. Luo, X. Wang, Y. Wang and L. Li, *J. Mater. Chem. A*, 2014, **2**, 510–519.
33 P. Hu, Y. Song, H. Liu, Y. Shen, Y. Lin and C.-W. Nan, *J. Mater. Chem. A*, 2013, **1**, 1688–1693.
34 S. P. Fillery, H. Koerner, L. Drummy, E. Dunkerley, M. F. Durstock, D. F. Schmidt and R. A. Vaia, *ACS Appl. Mater. Interfaces*, 2012, **4**, 1388–1396.
35 Z. M. Dang, H. Y. Wang, Y. H. Zhang and J. Q. Qi, *Macromol. Rapid Commun.*, 2005, **26**, 1185–1189.
36 L. L. Sun, B. Li, Y. Zhao, G. Mitchell and W. H. Zhong, *Nanotechnology*, 2010, **21**, 305702.
37 X. He, K. Yao and B. K. Gan, *J. Appl. Phys.*, 2005, **97**, 084101.
38 L. Xie, X. Huang, K. Yang, S. Li and P. Jiang, *J. Mater. Chem. A*, 2014, **2**, 5244–5251.
39 K. Yu, Y. Niu, Y. Zhou, Y. Bai and H. Wang, *J. Am. Ceram. Soc.*, 2013, **96**, 2519–2524.
40 B. Chu, M. Lin, B. Neese and Q. Zhang, *J. Appl. Phys.*, 2009, **105**, 014103.
41 X. Hao, J. Zhai and X. Yao, *J. Am. Ceram. Soc.*, 2009, **92**, 1133–1135.
42 K. Yang, X. Huang, L. Xie, C. Wu, P. Jiang and T. Tanaka, *Macromol. Rapid Commun.*, 2012, **33**, 1921–1926.

